Anharmonicity-induced excited-state quantum phase transition in the symmetric phase of the two-dimensional limit of the vibron model

Jamil Khalouf-Rivera, Francisco Pérez-Bernal, and Miguel Carvajal*

Departamento de Ciencias Integradas y Centro de Estudios Avanzados en Física, Matemáticas y Computación, Unidad Asociada GIFMAN CSIC-UHU, Universidad de Huelva, Huelva 21071, Spain and Instituto Carlos I de Física Teórica y Computacional, Universidad de Granada, Granada 18071, Spain

(Received 30 July 2021; accepted 16 March 2022; published 30 March 2022)

In most cases, excited-state quantum phase transitions can be associated with the existence of critical points (local extrema or saddle points) in a system's classical limit energy functional. However, an excited-state quantum phase transition might also stem from the lowering of the asymptotic energy of the corresponding energy functional. One such example occurs in the two-dimensional (2D) limit of the vibron model, once an anharmonic term in the form of a quadratic bosonic number operator is added to the Hamiltonian. This case has been studied in the broken-symmetry phase [Pérez-Bernal and Álvarez-Bajo, Phys. Rev. A **81**, 050101 (2010)]. In the present work we delve further into the nature of this excited-state quantum phase transition and we characterize it in the symmetric phase of the model, making use of quantities such as the effective frequency, the expected value of the quantum number operator, the participation ratio, the density of states, and the quantum fidelity susceptibility. In addition to this, we extend the usage of the quasilinearity parameter, introduced in molecular physics, to characterize the phases in the spectrum of the anharmonic 2D limit of the vibron model and a practical analysis is included with the characterization of the critical energies for the linear isomers HCN and HNC.

DOI: 10.1103/PhysRevA.105.032215

I. INTRODUCTION

Quantum phase transitions (QPTs) are zero-temperature phase transitions that occur when the ground state of a given quantum system undergoes an abrupt variation once a Hamiltonian parameter, a *control parameter*, goes through a critical value. Such transitions have been observed in numerous quantum systems and in different fields: quantum optics, condensed-matter physics, and atomic, nuclear, and molecular systems [1]. In algebraic models, based on Lie algebras and useful in studies of molecular [2,3], nuclear [4], and hadronic structure [5], the different phases can be mapped to the model dynamical symmetries. A general classification of ground-state QPTs in algebraic models can be found in [6] and for an extended treatment see the reviews in [7–9] and references therein.

The abrupt variation that characterizes a QPT is only fully realized in the large-system-size limit (also called thermodynamic or mean-field limit). However, for finite system sizes, the critical point can be identified by the appearance of QPT precursors in the form of sharp changes in several quantities, e.g., an energy gap collapse between consecutive levels, an increase in the energy density, or sudden changes in the participation ratio or the Wehrl entropy [10–15].

More recently, the study of QPTs has been extended to the realm of excited states, with the excited-state quantum phase transitions (ESQPTs) [16–18]. In ESQPTs, for a fixed value of the control parameter, a nonanalyticity in a certain derivative of the density of energy levels is found at a critical energy value [19–23]. Eigenstates below and above the critical energy are considered to belong to different phases. Therefore, ESQPTs can be accessed in two different ways: (i) varying the control parameter and tracing the changes of a given eigenstate once it goes through the critical energy value or (ii) fixing the control parameter and examining the properties of eigenstates at increasing energy values. Excited-state QPTs have been studied in different models, e.g., the nuclear interacting boson model [8], the kicked-top model [24], the Tavis-Cummings, Rabi, and Dicke [11,25–32] models, and the Lipkin-Meshkov-Glick model [8,33–37]. For a recently published complete review of the ESQPT field, see Ref. [23].

It is worth emphasizing that the bending vibration of nonrigid molecules is the first physical system where ESQPT signatures have been identified in experimental data [38–40]. In these cases, most fits have been performed within the two-dimensional limit of the vibron model (2DVM) using Hamiltonians that include up to two-body interactions. Considering the advances in molecular spectroscopy and the accuracy of the observed vibrational spectra, we recently obtained satisfactory results using an extended Hamiltonian including up to four-body interactions [41]. Other systems where signatures of ESQPTs have been detected in experimental results are superconducting microwave billiards [42] and spinor Bose-Einstein condensates [43]. In the latter case, recently published works include some promising developments [44,45].

Using as a starting point the results presented in Ref. [46] for the broken-symmetry phase, the study of ESQPTs in an anharmonic 2DVM Hamiltonian is extended to the symmetric

*miguel.carvajal@dfa.uhu.es

phase. The consideration of anharmonic terms is instrumental in the description of phase transitions and other physical phenomena in many systems. A limited set of examples includes the transition to chaos in the Fermi-Pasta-Ulam model [47,48], the description of nuclear critical shape phase transitions [49], the vibrational properties of solids [50], and the transition from normal to local vibrational modes in molecules [51–53].

In particular, we pay heed to the ESQPT in the symmetric phase, induced by an anharmonic term in the 2DVM Hamiltonian. This transition can be explained by changes in the phase-space boundary of the classical energy functional of the system obtained using the coherent state formalism. We compute several quantities that allow for the identification of the ESQPT critical energy such as the effective frequency, the expectation value of the quantum number operator, the density of states, the participation ratio, and the quantum fidelity susceptibility. The last two quantities were not included in the study of the broken-symmetry phase of Ref. [46]. For the sake of completeness, in addition to results for the symmetric phase, we also include results for the broken-symmetry phase.

The rest of this paper is organized as follows. In Sec. II we briefly outline the main results for the ground- and excited-state quantum phase transitions in a model Hamiltonian including an anharmonic term. We analyze the classical limit of the model, which allows us to obtain explicit expressions for the separatrix lines that mark the critical energies of the ESQPTs. Section III emphasizes the anharmonicity-induced ESQPT at the symmetric phase region. Nevertheless, we stress the connection with the symmetry-broken phase, aiming to have a complete description of the system ESQPTs. In addition to the characterization of the ESQPTs using the above-mentioned quantities, we introduce a quantity inspired by the molecular quasilinearity parameter that clearly marks the onset of each of the ESQPTs. In Sec. IV the previously presented results are applied to the bending degree of freedom of the linear isomers HCN and HNC. We summarize in Sec. V.

II. GROUND- AND EXCITED-STATE QUANTUM PHASE TRANSITIONS IN THE ANHARMONIC MODEL HAMILTONIAN OF THE 2DVM

In the present work we deal with the 2DVM, a two-dimensional approach introduced to model bending molecular vibrations as collective bosonic excitations (vibrons) [54]. The dynamical algebra of the system is u(3), with two dynamical symmetries, associated with the u(2) and so(3) subalgebras [38,54]. As a consequence of the conservation of the angular momentum component perpendicular to the plane of the bending motion, both chains end up in the system symmetry algebra so(2):

$$\begin{array}{ccccc} & & \mathrm{u}(2) & & \\ & \nearrow & & \searrow & \\ \mathrm{u}(3) & & & & \mathrm{so}(2). \\ & \searrow & & \nearrow & \\ & & \mathrm{so}(3) & & \end{array} \tag{1}$$

Each subalgebra chain provides a basis set and a solvable Hamiltonian that can be associated with a limiting physical case. In the molecular case, the u(2), or cylindrical oscillator chain, is associated with the bending degree of freedom for linear molecules. The states associated with this chain can be labeled as $|[N]n^{\ell}\rangle$, where $n = N, N-1, \ldots, 0$ is the vibrational quantum number and $\ell = \pm n, \pm(n-2), \ldots, \mathrm{mod}\,(n, 2)$ the vibrational angular momentum. The second chain, known as so(3) or a displaced oscillator chain, is linked with the bending of semirigid bent molecules. In this chain, the states are expressed as $|[N]\omega, \ell\rangle$, with branching rules $\omega = N, N-2, \ldots, \mathrm{mod}(N, 2)$ and $\ell = \pm\omega, \pm(\omega-1), \ldots, 0$, which are connected with the bending quantum number v_b and the figure axis projection K of the total angular momentum J of bent molecules by the relation $v_b = \frac{N-\omega}{2}$ and $K = \ell$. Additionally, the quantum numbers n and v_b are connected by the formula $n = 2v_b + |\ell|$.

The 2DVM encompasses all possible situations between the two previous limiting cases [55,56]. This can be evinced using a very simple Hamiltonian, with only two interaction terms: the first-order Casimir of u(2), $\hat{n}$, and the pairing operator $\hat{P} = N(N+1) - \hat{W}^2$, where N is the system size and $\hat{W}^2$ is the second-order Casimir of the so(3) subalgebra [38],

$$\hat{\mathcal{H}} = (1-\xi)\hat{n} + \frac{\xi}{N-1}\hat{P}. \tag{2}$$

We set to unity the overall energy scale and the control parameter $\xi \in [0, 1]$ takes the system from one limit to the other. Since the Hamiltonian (2) commutes with the operator $\hat{\ell}$, the vibrational angular momentum is conserved. The calculations in the present work are carried out in the u(2) basis $|[N]n^{\ell}\rangle$, which, for the sake of brevity, is shortened to $|n^{\ell}\rangle$.

The ground state of the system abruptly changes when going through the critical value $\xi_c = 0.2$ of the control parameter, where the system experiences a second-order ground-state QPT [38]. If $\xi = 0$, the Hamiltonian (2) is reduced to a truncated two-dimensional harmonic oscillator that is a convenient first approximation to bending vibrations for linear molecules. When $\xi = 1$, the model Hamiltonian has an anharmonic spectrum with a Goldstone mode that is suitable for modeling semirigid bent molecules. In the symmetric phase, for $\xi \in [0, \xi_c]$, the spectrum has a positive anharmonicity, a typical signature of quasilinear bending vibrations. The classical limit of the Hamiltonian at the critical point is a purely quartic potential [38]. In the broken-symmetry phase, for $\xi \in (\xi_c, 1]$, the spectrum is more complex, including the main features that characterize the bending of nonrigid and semirigid molecular species. Therefore, the 2DVM can tackle the feature-rich large-amplitude bending spectrum of nonrigid species [55,56]. This approach has also been used to model coupled benders [57–59] or the coupling between bending and stretching degrees of freedom [60–63].

The 2DVM is the simplest two-level model with a nontrivial angular momentum. This explains why it has been instrumental in the definition of ESQPTs from the onset [18]. Another relevant aspect regarding the 2DVM is the connection between quantum monodromy and the ESQPT [38]. The ESQPT appears in the broken-symmetry phase, where excited energy levels undergo a bent-to-linear transition for increasing energy values. An explicit expression of the separatrix line, which marks the energy with a high local density of states, can be obtained from the classical bending energy functional obtained using the coherent state formalism [38].

The bending spectrum in this parameter range $\xi \in (0.2, 1]$ presents signatures associated with the vibrations of nonrigid molecules, characterized by the existence of a barrier to linearity in the bending potential low enough to be straddled by excited states. This results in a large-amplitude bending mode and a feature-rich spectroscopy [64], with a sign-changing anharmonicity (Dixon dip [65]) and a dependence of energy on vibrational angular momentum that changes from quadratic to linear as the excitation energy goes through the barrier to linearity [39,66,67]. Mexican hat–or Champagne bottle–type potentials have been used for the modeling of nonrigid species, and the presence of the barrier to linearity prevents the definition of a set of globally valid action-angle variables [68]. When this classical feature is translated into the quantum realm, the result is quantum monodromy, which precludes the definition of a unique set of vibrational quantum numbers globally valid for the system [66,69]. Taking into consideration quantum monodromy simplifies the assignment of quantum labels to experimental bending levels in nonrigid molecular species [67,70–75].

Anharmonicity is included from the onset in the 2DVM, but the fit to experimental bending term values implies the explicit use of anharmonic corrections like the one considered in this work, $\hat{n}(\hat{n}+1)$. Thus, we consider the same Hamiltonian as in Ref. [46]: a 2DVM model Hamiltonian (2) plus a two-body interaction $\hat{n}(\hat{n}+1)$ with its corresponding control parameter α,

$$\hat{H} = (1-\xi)\hat{n} + \frac{\alpha}{N-1}\hat{n}(\hat{n}+1) + \frac{\xi}{N-1}\hat{P}, \tag{3}$$

where we scale the anharmonic interaction by a factor $N-1$ to transform the Hamiltonian into a form that allows for a convenient calculation of results in the large-size (mean-field) limit. The matrix elements of the Hamiltonian (3) in the u(2) basis are

$$\begin{aligned}\langle n_2^\ell|\hat{\mathcal{H}}|n_1^\ell\rangle = &\left\{(1-\xi)n_1 + \frac{\alpha}{N-1}n_1(n_1+1) + \frac{\xi}{N-1}[N(N+1) - (N-n_1)(n_1+2) - (N-n_1+1)n_1 - \ell^2]\right\}\delta_{n_2,n_1}\\ &+ \frac{\xi}{N-1}\sqrt{(N-n_1+2)(N-n_1+1)(n_1+\ell)(n_1-\ell)}\,\delta_{n_2,n_1-2}\\ &+ \frac{\xi}{N-1}\sqrt{(N-n_1)(N-n_1-1)(n_1+\ell+2)(n_1-\ell+2)}\,\delta_{n_2,n_1+2}.\end{aligned} \tag{4}$$

The addition of higher-order interactions to the model Hamiltonian (2) substantially modifies the model ESQPT. In Ref. [46] it was shown that the inclusion of the $\hat{n}(\hat{n}+1)$ term in the broken-symmetry phase $\xi \in (0.2, 1]$ induces a second critical energy and the corresponding separatrix line, marked by a high excited-state level density. Recently, in the framework of a study of the transition state in isomerization reactions [76], we noticed that the inclusion of the anharmonic term $\hat{n}(\hat{n}+1)$ with a negative parameter in the Hamiltonian triggers an ESQPT in the symmetric region too. The main motivation for the present work is to fully understand the ESQPT associated with the anharmonic term that, contrary to the case associated with the barrier to linearity and quantum monodromy, is not due to the existence of a saddle point or a local maximum in the energy functional obtained in the classical limit of the model [41]. This ESQPT can be traced back to changes in the phase-space boundary of the system's finite-dimensional Hilbert space [22,23,27]. In the case of Ref. [27], the so-called static ESQPTs were found at the edge of phase space for radiation-matter interaction models (Tavis-Cummings and Dicke models). However, as we will make clear below, the ESQPT related to anharmonicity is not a static one, as it has a singularity in the level density that will translate into significant effects for the system dynamics.

As in the broken-symmetry phase [46], the relevant features appear only for negative values of the α parameter. We depict in Fig. 1 the excitation energy for states with vibrational angular momenta $\ell = 0$ (blue solid line) and 1 (red dashed line) versus the control parameter ξ for $\alpha = -0.6$ and $N = 100$. Both ESQPT separatrices are characterized by a large local density of excited states and are marked in the figure with yellow dashed lines. The first ESQPT only occurs for $\xi > \xi_c = 0.2$, in the broken-symmetry phase. The second one, associated with the anharmonic term, can be present in the full ξ control parameter range.

The energy functional of the system's Hamiltonian (3) has been obtained in the mean-field limit using the number-projected coherent (or intrinsic) state approach and normalizing by the system size [38,46].

$$\mathcal{E}(r) = (1-\xi)\frac{r^2}{1+r^2} + \alpha\frac{r^4}{(1+r^2)^2} + \xi\left(\frac{1-r^2}{1+r^2}\right)^2 \tag{5}$$

The energy functional (5) for $\alpha = -0.6$ and several ξ values is shown in the insets of Fig. 1 with different colors. The corresponding spectrum in the correlation energy diagram is marked by a vertical dashed line of the same color. It can be noted that the energy functional transforms from a functional with a minimum at $r = 0$ (symmetric phase) into one with a minimum at $r \neq 0$ and a maximum at the origin (broken-symmetry phase) as the ξ value goes through the critical value $\xi_c = 0.2$. The larger the absolute value of the anharmonicity parameter α, the larger the decrease of the asymptotic value of the classical energy functional $\mathcal{E}(r)$. In the particular case of $\xi = 0.0$ (top left inset of Fig. 1), a maximum appears out of the origin above the asymptotic value. This case is explained below and, as a consequence, a threshold value of α is defined to avoid this situation. For a given α, there is a ξ value for which the two separatrices cross. In this case, the maximum at the origin and the asymptotic energy functional value $\lim_{r\to\infty}\mathcal{E}(r)$ are equal. From this ξ value on,

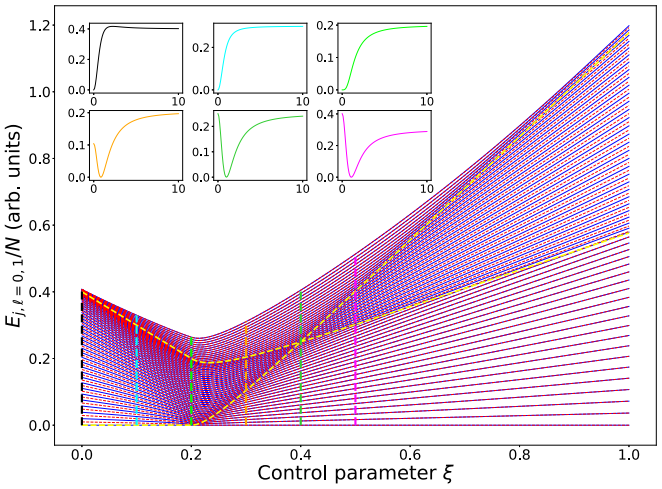

FIG. 1. Normalized excitation energy $E_{j,\ell}$, in arbitrary units, for states with vibrational angular momentum $\ell = 0, 1$, as a function of the control parameter ξ for $\alpha = -0.6$ and a system size $N = 100$. The $\ell = 0$ (1) energies are depicted using blue solid (red dashed) lines. The yellow dashed lines are the two ESQPT separatrices calculated in the mean-field limit. The insets (from top to bottom and left to right) provide the energy functionals of the system's Hamiltonian $\mathcal{E}(r)$, setting their minima to zero, corresponding to the vertical colored dashed lines at $\xi = 0.0$, 0.1, 0.2, 0.3, 0.4, and 0.5 (from left to right, black, light blue, light green, orange, dark green, and pink, respectively)

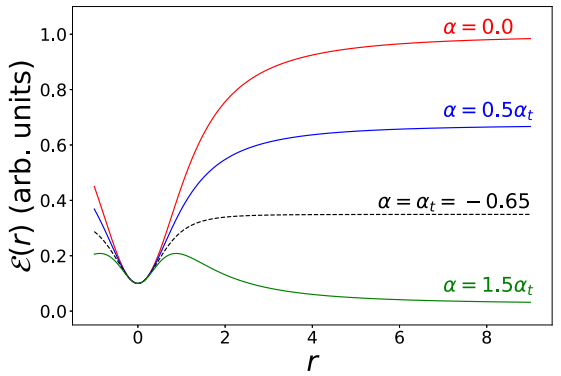

FIG. 2. Energy functionals for the Hamiltonian of Eq. (3) with a control parameter $\xi = 0.1$ and α values 0 (red line), $0.5\alpha_t$ (blue line), α_t (black dashed line), and $1.5\alpha_t$ (green line). All quantities are unitless.

the energy functional at the origin is larger than its asymptotic value.

A Landau analysis of the ground-state QPT for the model Hamiltonian (2) was performed in Ref. [38] and for the Hamiltonian with the anharmonic term in Ref. [46]. In the latter case, the analysis was limited to the bent or broken-symmetry phase, where two ESQPTs occur. The equations for the separatrices in the broken-symmetry phase (yellow dashed lines in Fig. 1), $f_1(\xi, \alpha)$ and $f_2(\xi, \alpha)$, provide the normalized critical excitation energy for each ESQPT and were published in Ref. [46]. In the present work, an analysis of the classical energy functional is carried out to define the continuation of the broken-symmetry phase separatrix $f_2(\xi, \alpha)$ in the symmetric phase. Thus the equations for the two separatrices along the full ξ range, $\xi \in [0, 1]$, are

$$f_1(\xi, \alpha) = \mathcal{E}(r = 0) - \mathcal{E}(r = r_{\min}) = \frac{(5\xi - 1)^2}{4(4\xi + \alpha)} \quad \text{if } \xi > \xi_c, \tag{6}$$

$$\begin{aligned} f_2(\xi, \alpha) &= \mathcal{E}(r \to \infty) - \mathcal{E}(r = r_{\min}) \\ &= \begin{cases} \mathcal{E}(r \to \infty) - \mathcal{E}(r = 0) = 1 + \alpha - \xi, & \xi \leqslant \xi_c \\ \mathcal{E}(r \to \infty) - \mathcal{E}(r = r_{\min}) = \frac{(1+2\alpha+3\xi)^2}{4(4\xi+\alpha)}, & \xi > \xi_c, \end{cases} \end{aligned} \tag{7}$$

where $r_{\min} = \sqrt{\frac{5(\xi - \xi_c)}{2\alpha + (3\xi + 1)}}$ is the r value associated with a minimum in the broken-symmetry phase. The first separatrix $f_1(\xi, \alpha)$ is the relative height of the barrier to linearity (maximum in the origin of the energy functional) and the second one $f_2(\xi, \alpha)$ is the difference between the asymptotic value of the energy functional and its minimum [46]. In the present work we consider also the symmetric phase $\xi \in [0, \xi_c]$, where there can be only one separatrix line $f_2(\xi, \alpha)$, defined as the energy difference between the minimum of the energy functional, located at $r = 0$ in this phase, and its asymptotic value (see Fig. 1). Therefore, as can be easily seen in Eq. (7), the $f_2(\xi, \alpha)$ separatrix is a continuous function of ξ, albeit its first derivative is discontinuous at $\xi = \xi_c$.

In Fig. 1 it can be clearly seen how the ground-state QPT occurs at $\xi = \xi_c = 0.2$, where the onset of the bent-to-linear ESQPT is also located, marked by its associated separatrix $f_1(\xi, \alpha)$. At higher-energy values, the ESQPT associated with the anharmonicity and its separatrix $f_2(\xi, \alpha)$ defines a second region of high density of states that is also present in both the symmetric and broken-symmetry phases. Separatrix lines denote critical energies at which states with different vibrational angular momenta can be degenerate or the degeneracy can be broken. In the symmetric phase, eigenstates with different angular momenta below the $f_2(\xi, \alpha)$ separatrix are nondegenerate and become degenerate above the critical energy. In the broken-symmetry phase and before the crossing of separatrices, states at energies below the $f_1(\xi, \alpha)$ and above the $f_2(\xi, \alpha)$ separatrix are degenerate. This is reversed after the crossing and the degeneracy is broken for states in between both separatrices.

A threshold value of α in the symmetric region, α_t, can be obtained by applying the maximum condition to the energy functional (5) out of the origin ($r \neq 0$):

$$\left.\frac{\partial \mathcal{E}(r)}{\partial r}\right|_{r \neq 0} = 0 \longrightarrow r^2 = \frac{5(\xi - \xi_c)}{2\alpha + (3\xi + 1)}. \tag{8}$$

We can compute a minimum value of the negative parameter α by imposing that there is no other extreme but the one in the origin, which translates into a lower bound in the value of the control parameter: $\alpha \geqslant \alpha_t$. As we are interested in the range $\xi \in [0, \xi_c]$, the numerator of (8) is zero or negative. Hence, we impose the condition $2\alpha + (3\xi + 1) > 0$, obtaining a threshold value $\alpha_t = -\frac{3\xi+1}{2}$. Therefore, the range of α values with a single minimum at the origin that characterizes the bending vibration in linear and quasilinear molecular configurations is given by $\alpha \geqslant -\frac{3\xi+1}{2}$. This is shown in Fig. 2, where we depict

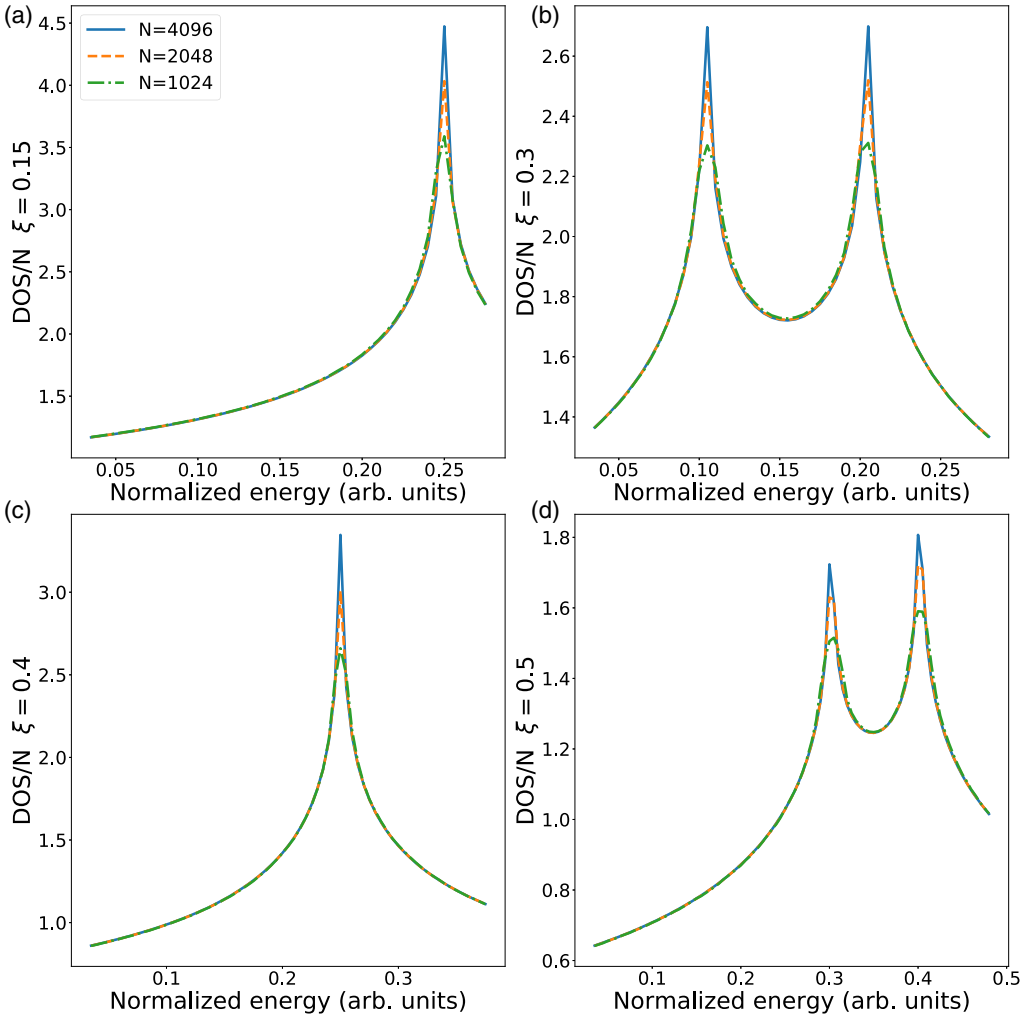

FIG. 3. Density of vibrational angular momentum $\ell = 0$ states (DOS) for $\alpha = -0.6$ and (a) $\xi = 0.15$, (b) 0.3, (c) 0.4, and (d) 0.5. Each case is computed for system size values $N = 1024$, 2048, and 4096. All quantities are unitless.

various energy functionals (5) for $\xi = 0.1$ and different α values. Apart from the threshold value α_t (black dashed line), the $\alpha = 0$ (red line), $0.5\alpha_t$ (blue line), and $1.5\alpha_t$ (green line) cases are depicted. In this figure it can be clearly seen that the main outcome of the anharmonic operator in the model classical limit is to shift the asymptotic potential value. If the anharmonicity were positive, the asymptotic value would increase without an associated ESQPT. However, for negative α, the asymptotic energy functional value happens at lower energies. If $\alpha < \alpha_t$, a maximum at $r \neq 0$ appears and the asymptotic energy could be the minimum energy and become the ground state of the system, e.g., the green line in Fig. 2, where $\alpha = 1.5\alpha_t$.

In the present work we only address the case $\alpha \in [\alpha_t, 0]$, which has been found a realistic approach in the study of highly excited states of linear molecules in the presence of bond-breaking isomerization [76]. Therefore, for the range of α values under consideration, the asymptotic value of the energy functional (5) becomes the $f_2(\xi, \alpha)$ separatrix that characterizes the second ESQPT. Nevertheless, the second-order QPT is basically unaffected by this addition and it is still occurring at $\xi_c = 0.2$ [46]. A similar situation occurs in the anharmonic Lipkin-Meshkov-Glick model [77–79]. As previously mentioned, the anharmonic 2DVM symmetric phase provides a case in point of the occurrence of an ESQPT without an associated QPT. In systems with more than one control parameter, there are other examples of ESQPTs without an associated QPT that can be traced back to critical points in particular trajectories in the parameter space [80–82]. In the present case, as can be seen in the energy functionals in Fig. 2, the control parameter α varies the asymptotic value of the functional instead of generating new critical points. This is a fine example of an ESQPT induced by the boundary of a finite Hilbert space [23].

As previously mentioned, the $f_1(\xi, \alpha)$ and $f_2(\xi, \alpha)$ separatrices in Fig. 1 denote the critical ESQPT energies, characterized by a high density of excited states. In Fig. 3 we depict the density of $\ell = 0$ states calculated numerically versus the normalized energy for $N = 1024$, 2048, and 4096; $\alpha = -0.6$; and $\xi = 0.15$ (symmetric phase) and $\xi = 0.3$, 0.4, and 0.5 (broken-symmetry phase). In the $\xi = 0.15$ case [Fig. 3(a)], the peak in the density of states can be traced back to the ESQPT associated with the anharmonicity. It can also be observed that for $\xi = 0.3$ and 0.5 [Figs. 3(b) and 3(d)], there

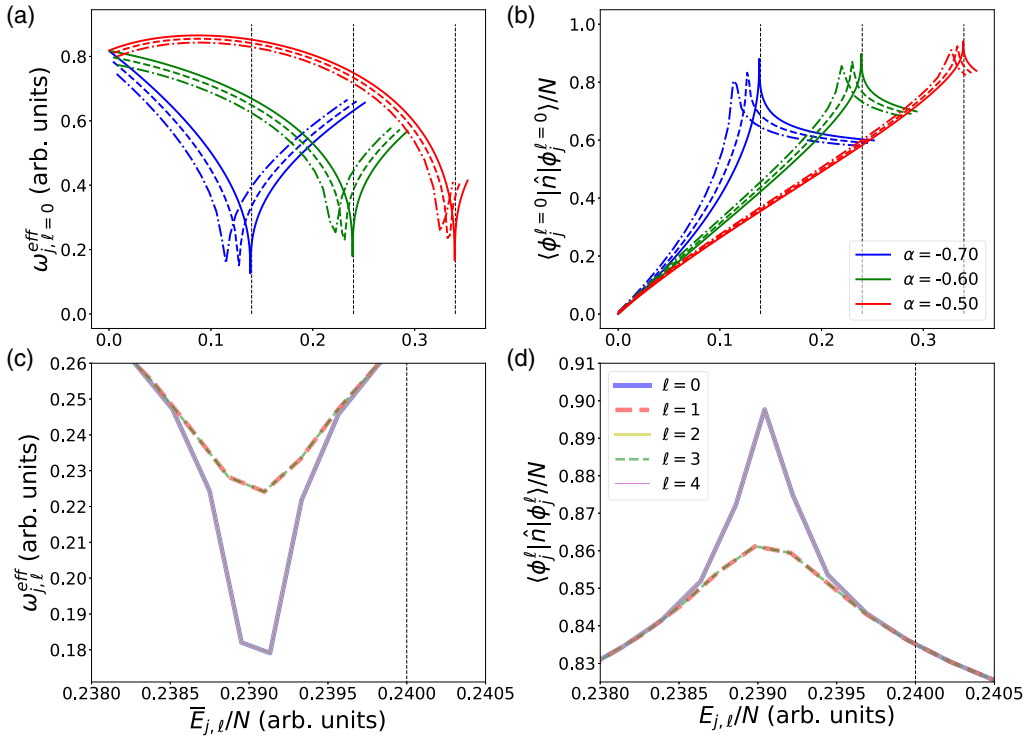

FIG. 4. (a) Effective frequency $\omega^{\text{eff}}_{j,\ell=0}$ versus the mean value of the normalized excitation energy for $\ell = 0$ states. (b) Expected value of $\hat{n}$ for the system with $\ell = 0$ eigenstates versus the normalized excitation energy. The calculations in both (a) and (b) are carried out for the Hamiltonian (3) with $N = 50$ (dot-dashed lines), 100 (dashed lines), and 1000 (solid lines); $\xi = 0.16$; and different α values [from left to right, $\alpha = -0.7$ (blue), -0.6 (green), and -0.5 (red)]. The thin vertical black dashed lines indicate the critical energy obtained in the mean-field limit. (c) and (d) Close-up of the results for the corresponding quantities in the $N = 1000$ and $\alpha = -0.6$ case depicted for various angular momentum values. In both (c) and (d) solid (dashed) lines are used for even (odd) angular momentum values. All depicted quantities are unitless.

are two peaks in the density of states, one for each separatrix. Finally, at the intersection of the separatrices, for $\xi = 0.4$, only one maximum occurs [Fig. 3(c)]. As expected, the larger the value of N, the higher the peaks in the density of states due to the logarithmic divergence associated with ESQPTs in the mean-field limit.

III. CHARACTERIZATION OF THE ANHARMONICITY-INDUCED EXCITED-STATE QUANTUM PHASE TRANSITION

The present section aims to characterize the anharmonicity-induced ESQPT in the symmetric phase region with the effective frequency, the expectation value of the number operator, the participation ratio, and the quantum fidelity susceptibility. In addition to this, a quantity inspired on the molecular quasilinearity parameter used to quantify molecular bending degrees of freedom as linear, quasilinear, or semirigid [64,83] is introduced to locate the different phases in the excited spectrum. This parameter was previously considered to characterize the ground-state quantum phase transition in the 2DVM [41].

The effective frequency [84], defined as the difference between adjacent levels $\Delta E_{j,\ell}$ divided by the number of quanta Δj, $\omega^{\text{eff}}_{j,\ell} = \Delta E_{j,\ell}/\Delta j$, allows for the characterization of ESQPTs, as well as the expectation value of the $\hat{n}$ operator in the Hamiltonian eigenstates. The latter quantity behaves as an order parameter for the ground-state QPT [38]. Both quantities are depicted in Fig. 4 for system sizes $N = 50$, 100, and 1000; control parameter $\xi = 0.16$; and anharmonicity parameter values $\alpha = -0.5$, -0.6, and -0.7. In Fig. 4(a), $\omega^{\text{eff}}_{j,\ell}$ is depicted versus the normalized mean excitation energy between adjacent states $[\overline{E}_{j,\ell} = (E_{j-1,\ell} + E_{j,\ell})/2]$, a plot that is akin to a Birge-Sponer diagram. In this figure, a deep minimum evinces the critical ESQPT energy. This minimum, in the transition to linearity, is the well-known Dixon dip [65]. The expectation value of $\hat{n}$ is depicted in Fig. 4(b) as a function of the normalized excitation energy, with peaks at the same critical energy values. Though these features grow sharper for larger system sizes, clear ESQPT precursors are found for low N values. As the value of N increases, the critical energy tends to the $f_2(\xi, \alpha)$ (7) values marked with vertical black dashed lines. The behavior of these two quantities agrees with the observed one in the broken-symmetry phase ($\xi > 0.2$) [46] when the system goes across the $f_2(\xi, \alpha)$ critical energy in the symmetric region ($\xi < 0.2$). In Figs. 4(c) and 4(d) the corresponding quantities are depicted for energies close to the critical energy and various angular momentum values for the $N = 1000$ and $\alpha = -0.6$ system. In both cases, staggering between even (solid lines) and odd (dashed lines) angular momenta is evinced. The explanation for this staggering requires the analysis of the wave-function structure in the vicinity of the critical energy, which is carried out with the participation ratio.

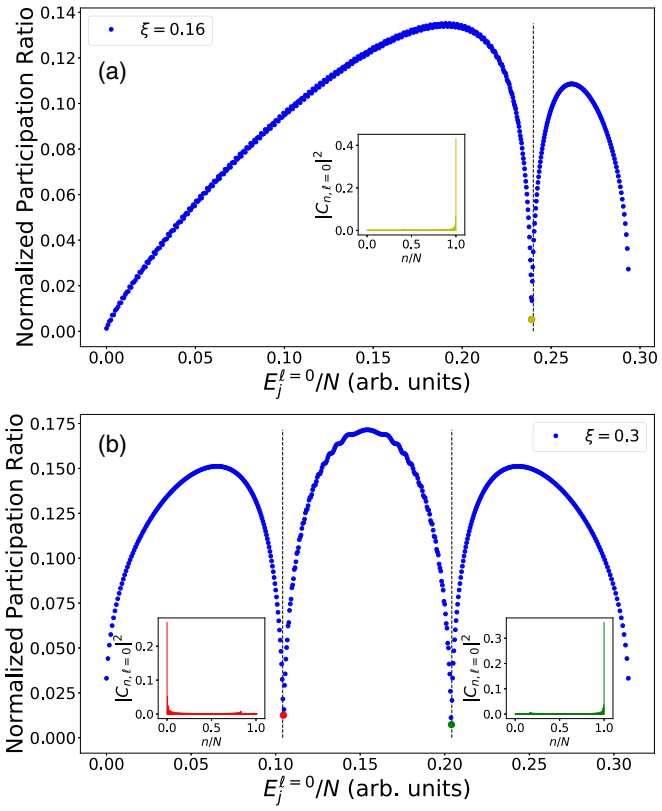

FIG. 5. Normalized PR for eigenstates expressed in the u(2) basis as a function of the normalized excitation energy for systems with $N = 1000$, $\alpha = -0.6$, and control parameters (a) $\xi = 0.16$ and (b) $\xi = 0.3$. The squared components of the wave functions in the u(2) basis versus n/N for the critical states are shown as bar graphs in three insets. The critical states are highlighted using the same color of the bar diagram [(a) yellow and (b) red (left) and green (right)]. The thin vertical black dashed lines indicate the critical energy obtained in the mean-field limit. All depicted quantities are unitless.

It has been shown for systems in one, two, and three dimensions that the eigenstates having energies close to the critical energy are strongly localized in the u(n) basis in ESQPTs associated with a u(n) − so($n+1$) ground-state quantum phase transition [85–87]. In the 2DVM case, the localization of a given state, expressed in the u(2) basis, $|\psi\rangle = \sum_{n,\ell} C_{n,\ell}|n^\ell\rangle$, can be assessed using the participation ratio (PR) [88] (also known as the inverse participation ratio [89] or number of principal components [90])

$$P(\psi) = \frac{1}{\sum_{n,\ell} |C_{n,\ell}|^4}. \tag{9}$$

In the ESQPT associated with the barrier to linearity, the states with energies close to the critical energy are strongly localized when expressed in the u(2) chain basis in the state of the basis with the lowest value of n ($n = \ell$ for a given ℓ block). For $\ell = 0$, the largest weight corresponds to the $|0^0\rangle$ component [41,87,91].

We plot in Fig. 5 the normalized PR versus the normalized excitation energy for Hamiltonian (3) eigenstates with $\ell = 0$, $\xi = 0.16$ [Fig. 5(a)] and 0.3 [Fig. 5(b)], $\alpha = -0.6$, and a system size $N = 1000$. The lower the PR value, the higher the state localization. As expected, states close to the spectrum edges are well located in the u(2) basis. In the system with $\xi = 0.16$ [Fig. 5(a)], a minimum PR value occurs for states with energies close to the ESQPT critical energy. The critical energy computed in the mean-field limit, $f_2(\xi, \alpha)$, is marked with a black dashed line. The state with the minimum value of the PR and closest to the critical energy is highlighted with a yellow point and the squared coefficients $|C^j_{n,\ell}|^2$ of its wave function are displayed in the inset as a function of the normalized quantum number n/N. In particular, as it was already noticed in Ref. [76], the localization is achieved in the u(2) basis state with a maximum n value, which corresponds to $n = N = 1000$ in this case.

In Fig. 5(b) a case in the broken-symmetry phase ($\xi = 0.3$) for $\ell = 0$ is included. For this value of the control parameter, the system goes through both ESQPTs. The first one corresponds to the transition to linearity and the state with a minimum value of the PR (highlighted with a red point) is well localized in the first state of the basis $|0^0\rangle$, as expected [41,87,91] (see the left inset, where the squared components of the wave function are plotted as a function of n/N). The second ESQPT is due to the anharmonic term. In this case, the state with a minimum value of the PR is marked with a green point and, as we showed in the symmetric phase, its wave function is localized in the $|N^{\ell=0}\rangle$ state (see the right inset, where we display the squared coefficients of the wave function versus n/N).

The structure of the wave function for states close to the critical energy of the anharmonicity-induced ESQPT explains the staggering between results for odd and even angular momenta shown in Figs. 4(c) and 4(d). Assuming N is even and even (odd) values of the angular momentum, the state close to the critical energy are localized in $|N^\ell\rangle$ ($|N-1^\ell\rangle$), which is the state of the u(2) basis with the largest possible n value. In both cases, the staggering is reversed when an odd value of N is considered, and the largest changes occur for odd angular momenta.

Following Ref. [91], we use the quantum fidelity susceptibility (QFS) as an ESQPT marker. The quantum fidelity, initially introduced in the field of quantum information, is defined as the module of the overlap between two quantum states [92]. It was later extended to the study of QPTs [93,94]. In the latter case, for a λ control parameter, the fidelity is computed as $F(\lambda, \delta\lambda) = |\langle\phi^\ell_j(\lambda)|\phi^\ell_j(\lambda+\delta\lambda)\rangle|$. This quantity can be used to characterize QPTs, though it has the drawback of being dependent on the $\delta\lambda$ value. This can be overcome using the QFS $\chi_F(\lambda)$, defined as minus the second derivative of $F(\lambda, \delta\lambda)$ with respect to the perturbation $\delta\lambda$, which is the leading term in the series expansion of the quantum fidelity as a function of $\delta\lambda$ [94,95]. In this case, if the system Hamiltonian is expressed as $\hat{H}(\lambda) = \hat{H}_0 + \lambda\hat{H}^I$, the QFS for the jth system state can be computed as

$$\chi_F^{(j)}(\lambda) = \sum_{i\neq j}^{\dim} \frac{|\langle\phi_i(\lambda)|\hat{H}^I|\phi_j(\lambda)\rangle|^2}{[E_i(\lambda) - E_j(\lambda)]^2}, \tag{10}$$

where $|\phi_i(\lambda)\rangle$ and $E_i(\lambda)$ are the ith eigenstate and eigenvalue, respectively. We have introduced this approach for the characterization of ESQPTs in the 2DVM [91] and it has also been used recently in the study of the chaotic regime of spin chain

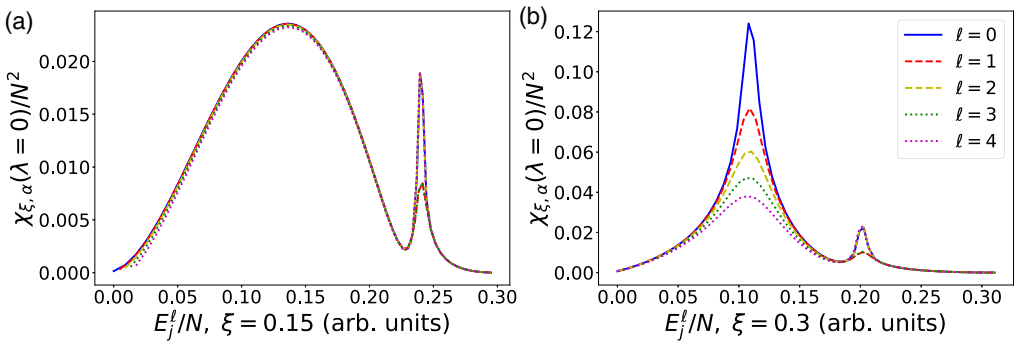

FIG. 6. Quantum fidelity susceptibility $\chi_F^{(j)}(\lambda=0)$ as a function of the normalized energy for eigenstates with $\ell=0$ (blue solid line), 1 (red dot-dashed line), 2 (yellow dashed line), 3 (green dotted line) and 4 (fuchsia dotted line) and a system size $N=100$. The control parameters are $\alpha=-0.6$ and (a) $\xi=0.16$ and (b) $\xi=0.3$. All depicted quantities are unitless.

models [96] and the adiabatic and counteradiabatic driving in ESQPTs [23].

Using the approach described in [91], we assign a weight $1-\lambda$ to the terms diagonal in the u(2) basis in the Hamiltonian (3) and $1+\lambda$ to the term diagonal in the so(3) basis

$$\hat{H}(\lambda)=(1-\lambda)\left[(1-\xi)\hat{n}+\frac{\alpha}{N-1}\hat{n}(\hat{n}+1)\right]+(1+\lambda)\left[\frac{\xi}{N-1}\hat{P}\right], \tag{11}$$

where $\hat{H}^I$ is the interaction Hamiltonian, which in the present case is

$$\hat{H}^I=-\left[(1-\xi)\hat{n}+\frac{\alpha}{N-1}\hat{n}(\hat{n}+1)\right]+\frac{\xi}{N-1}\hat{P}.$$

The obtained results are depicted in Fig. 6 for two different values of ξ, 0.16 [Fig. 6(a)] and 0.3 [Fig. 6(b)], $\alpha=-0.6$, and $N=100$ as a function of the normalized excitation energy for the eigenstates of a system with $\lambda=0$. Different values of the vibrational angular momentum ℓ, 0 (blue solid line), 1 (red solid line), 2 (yellow dashed line), 3 (green dotted line), and 4 (fuchsia dotted line), are considered.

In the case of $\xi=0.16$ [Fig. 6(a)], there are two maxima. The first one is a smooth maximum at values in the range (0.05, 0.20), which can be explained by the QFS shape in the symmetric phase for cases with $\alpha=0$. The second maximum is steeper and is localized in the vicinity of the anharmonicity-induced ESQPT critical energy. In the plot, this maximum takes two different values depending on the parity of the angular momentum, being lower for odd ℓ values. This staggering can be again explained by taking into account that states close to this ESQPT critical energy are localized in the $u(2)$ basis state with the maximum possible n value, $n=N$ ($n=N-1$) for even (odd) values of the angular momentum, assuming an even value of the total boson number N. As with the previous quantities, we check that for an odd N value, the staggering is reversed.

In Fig. 6(b) we show the QFS for a system with $\xi=0.3$. In this case, the lower energy maximum is due to the transition to linearity. As was anticipated [18,41,87,91], the precursors of this transition become softer as the vibrational angular momentum increases as a consequence of the centrifugal barrier hindering the system's exploration of the maximum in the origin. The second maximum is lower and displays the same staggering observed in the symmetric case $\xi=0.16$. Therefore, for large values of ℓ, ESQPT precursors are only presented for the anharmonicity-induced transition.

The last quantity we study can be traced back to the quasilinearity parameter for bending vibrations introduced by Yamada and Winnewisser [83]. The quasilinearity parameter aims to quantify the degree of quasilinearity in a bending vibration and it is defined as the ratio between the excitation energies of the first $\ell=1$ and $\ell=0$ excited states [64]. In this work this parameter is recast and is extended to the realm of excited states. This parameter is helpful in the identification of the critical energies for the two ESQPT in the anharmonic 2DVM. The generalization of the quasilinearity parameter introduced is

$$\gamma_{n,\ell}=\frac{E_{n+1,\ell+1}-E_{n,\ell}}{E_{n+2,\ell}-E_{n,\ell}}, \tag{12}$$

where it takes, for the ground state, the value 1/2 in the symmetric phase and 0 in the broken-symmetry phase. The labeling of the energy levels can also be expressed in the so(3) chain basis with (ν_b, K) quantum numbers, using the customary notation for bent molecules.

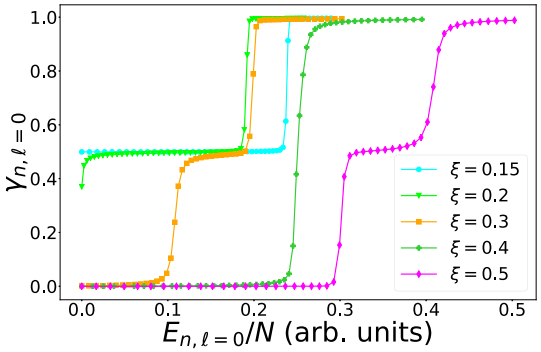

FIG. 7. Parameter $\gamma_{n,\ell=0}$ as a function of the normalized energy levels with vibrational angular momentum $\ell=0$ for $N=100$, $\alpha=-0.6$, and $\xi=0.15$, 0.2, 0.3, 0.4, and 0.5 (light blue, light green, orange, dark green, and pink, respectively). All depicted quantities are unitless.

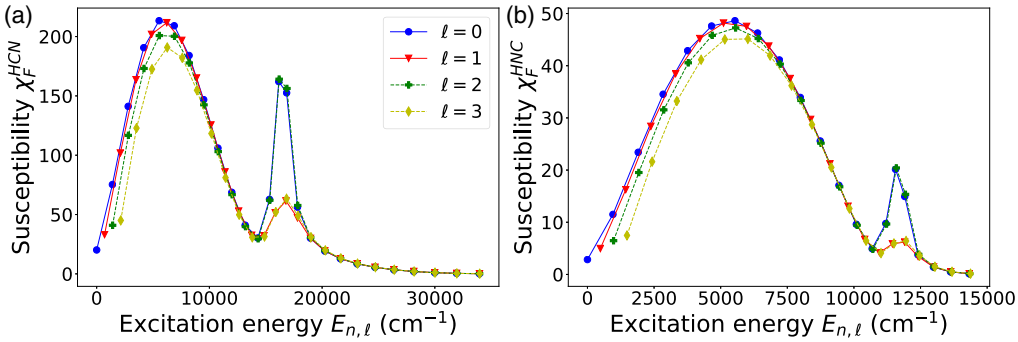

FIG. 8. Quantum fidelity susceptibility for states with vibrational angular momentum $\ell = 0$, 1, 2, and 3 for the (a) HCN and (b) HNC isomers.

In Fig. 7 we depict $\gamma_{n,\ell=0}$ as a function of the normalized excitation energy for the Hamiltonian (3) with $N = 100$, $\alpha = -0.6$, and various values of the control parameters ξ ($\xi = 0.15$, 0.2, 0.3, 0.4, and 0.5) using the same colors as in Fig. 1. It can be clearly seen in this figure how the $\gamma_{n,0}$ quasilinearity parameter identifies the ESQPT critical energies, changing abruptly as it straddles the critical energy of an ESQPT. In the symmetric phase $\xi = 0.15$, $\gamma_{n,0}$ presents a step from 0.5 to 1.0 when the system reaches the critical energy of the ESQPT associated with the anharmonicity. The value of $\gamma_{n,0}$ is 1 above of the anharmonicity-induced ESQPT, because the states $|n+1^{\ell+1}\rangle = |v_b, \ell+1\rangle$ and $|n+2^{\ell}\rangle = |v_b+1, \ell\rangle$ become degenerated. At $\xi_c = 0.2$, the behavior is similar, although signatures of the ground-state QPT are observed for low energies. In the broken-symmetry phase, the $\xi = 0.3$ and 0.5 cases, the parameter increases from 0.0 to 0.5 and from 0.5 to 1.0, as it reaches the critical energy of each one of the two ESQPTs. As in the symmetric phase, $\gamma_{n,0}$ is equal to 1.0 above the two ESQPT separatrices, because of the degeneration of the states $|n+1^{\ell+1}\rangle = |v_b, \ell+1\rangle$ and $|n+2^{\ell}\rangle = |v_b+1, \ell\rangle$. However, when $\gamma_{n,0} = 0.0$, the degenerate states are $|n+1^{\ell+1}\rangle = |v_b, \ell+1\rangle$ and $|n^{\ell}\rangle = |v_b, \ell\rangle$. The last value of the control parameter we consider is $\xi = 0.4$, when both separatrices cross. At the crossing energy, $\gamma_{n,0}$ increases from 0.0 to 1.0, as it is sensitive to the change in the way the states are degenerate. It is worth emphasizing that the quasilinearity parameter distinguishes between the two different phases and indicates the critical energy.

IV. APPLICATION TO THE LINEAR ISOMERS HCN AND HNC

As an application, an analysis of the anharmonicity-induced ESQPT is carried out for the bending degree of freedom of the two linear isomers HCN and HNC. In Ref. [76] it was shown that the anharmonicity-induced ESQPT in the symmetric phase for these two molecules is instrumental for reproducing the transition state energy for the isomerization between these two species. In this section the ESQPT critical points associated with the functional asymptotes are identified using the QFS and the $\gamma_{n,\ell}$ parameter for the two molecular species HCN and HNC. The predicted spectra and eigenfunctions for the two isomers are taken from Ref. [76], where $N = 50$ and 40 for HCN and HNC, respectively. Both molecular species are described using a more complex Hamiltonian considering up to four-body interactions, which allows for a more accurate modeling.

In Fig. 8 the QFS is calculated for the $\ell = 0$, 1, 2, and 3 energy levels of HCN [Fig. 8(a)] and HNC [Fig. 8(b)]. It can be observed that the behavior for both species is similar to the one obtained for the model Hamiltonian: A smooth maximum appears before the peak coming from the ESQPT associated with the anharmonicity. In both cases the first maximum decreases with ℓ, something that can be traced back to the influence of the centrifugal barrier. The ESQPT-associated peak has a noticeable staggering, with an approximately constant value for even ℓ values and odd ℓ values, the value being larger for the even angular momenta. This staggering can be explained as in the anharmonic model Hamiltonian. The ESQPT-related peaks in both cases occur at the energies associated with the isomerization transition state, in agreement with the results published in Ref. [76]. It is worth emphasizing how for low N values the ESQPT precursors can be clearly evinced.

The $\gamma_{n,\ell=0}$ parameter for the two species HCN and HNC is plot in Fig. 9 as a function of the excitation energy of the vibrational bending degree of freedom. As in the $\xi = 0.15$ case in Fig. 7, both molecules present an increase of the $\gamma_{n,\ell=0}$

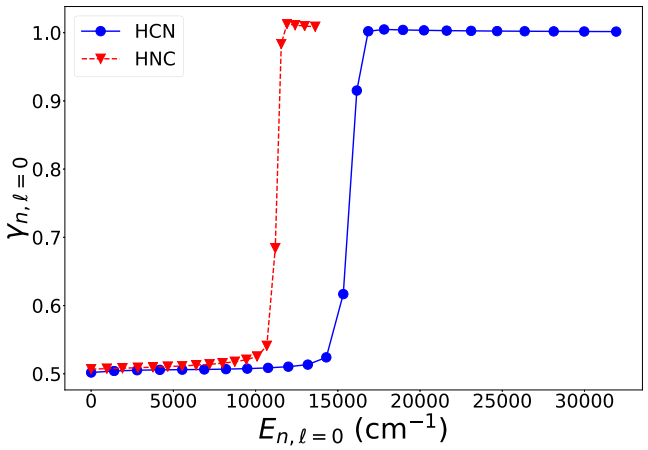

FIG. 9. Quasilinearity parameter $\gamma_{n,\ell=0}$ with respect to the excitation energy of the vibrational bending degree of freedom for HCN and HNC.

parameter from 0.5 to 1.0 as the excitation energy approaches the critical ESQPT energy, corresponding to the isomerization transition state for this system.

V. CONCLUSION

We have shown that the ESQPT associated with the inclusion of an anharmonic $\hat{n}(\hat{n}+1)$ term in the model Hamiltonian of the 2DVM is not limited to the broken-symmetry phase, as studied in [46], but it also extends to the symmetric phase. We have studied this situation for anharmonic parameters α over a threshold value and derived, using the intrinsic state formalism, the analytic dependence of the separatrix in this phase [see Eq. (7)]. We have depicted the ground-state QPT order parameter (the expectation value of $\hat{n}$) and the effective frequency plot (see Fig. 4) for different parameter values observing the ESQPT precursors. Using the resulting eigenfunctions, we have shown the high degree of localization in the u(2) basis of eigenstates with an energy close to the ESQPT critical energy (see Fig. 5) and we have studied the effect of the ESQPT over the QFS (see Fig. 6). For the ESQPT probes considered, we have explained the staggering observed for states close to critical energy with angular momentum of different parity.

Moreover, we suggested the use of a parameter inspired by the molecular quasilinearity parameter to denote the ESQPT presence as it abruptly changes when going through the critical energy of any ESQPT. We would like to emphasize that the ESQPT in the 2DVM symmetric phase is not related to the existence of critical points in the energy functional obtained in the classical limit of the system (local maxima or saddle points) but to the changes in the phase-space boundary brought by the anharmonic term.

In a recent work, using a Hamiltonian with higher-order interactions, we successfully used the anharmonicity-induced ESQPT to characterize the transition state in the HCN-HNC isomerization [76]. In this work the linear isomers HCN and HNC were taken as examples for the characterization of the anharmonicity-induced ESQPT without an associated QPT and the transition states were identified using QFS and the quasilinearity parameter.

ACKNOWLEDGMENTS

We acknowledge useful discussions with José Miguel Arias, Manuel Calixto, Pedro Pérez Fernández, and Lea Santos. This project received funding from the European Union's Horizon 2020 research and innovation program under Marie Skłodowska-Curie Grant Agreement No. 872081 and from Grant No. PID2019-104002GB-C21 funded by MCIN/AEI/10.13039/501100011033 and, as appropriate, by ERDF A way of making Europe, by the European Union, or by the European Union NextGenerationEU/PRTR. This work was also partially supported by the Consejería de Transformación Económica, Industria, Conocimiento y Universidades, Junta de Andalucía, and European Regional Development Fund through Grants No. UHU-1262561 (J.K.-R. and F.P.-B.) and No. PY2000764 and by the Ministerio de Ciencia, Innovación y Universidades (Grant No. COOPB20364) (M.C.). Computing resources supporting this work were provided by the CEAFMC and Universidad de Huelva High Performance Computer located at the Campus Universitario el Carmen and funded by FEDER/MINECO Project No. UNHU-15CE-2848.

[1] L. Carr, *Understanding Quantum Phase Transitions* (CRC, Boca Raton, 2010).
[2] F. Iachello and R. D. Levine, *Algebraic Theory of Molecules* (Oxford University Press, New York, 1995).
[3] A. Frank and P. Van Isacker, *Algebraic Methods in Molecular and Nuclear Structure Physics* (Wiley, New York, 1994).
[4] F. Iachello and A. Arima, *The Interacting Boson Model* (Cambridge University Press, Cambridge, 1987).
[5] R. Bijker, F. Iachello, and A. Leviatan, Algebraic models of hadron structure. i. nonstrange baryons, Ann. Phys. (NY) **236**, 69 (1994).
[6] P. Cejnar and F. Iachello, Phase structure of interacting boson models in arbitrary dimension, J. Phys. A: Math. Theor. **40**, 581 (2007).
[7] R. F. Casten, Quantum phase transitions and structural evolution in nuclei, Prog. Part. Nucl. Phys. **62**, 183 (2009).
[8] P. Cejnar and J. Jolie, Quantum phase transitions in the interacting boson model, Prog. Part. Nucl. Phys. **62**, 210 (2009).
[9] P. Cejnar, J. Jolie, and R. F. Casten, Quantum phase transitions in the shapes of atomic nuclei, Rev. Mod. Phys. **82**, 2155 (2010).
[10] Y. Zhang, F. Pan, Y.-X. Liu, and J. P. Draayer, The $E(2)$ symmetry and quantum phase transition in the two-dimensional limit of the vibron model, J. Phys. B **43**, 225101 (2010).
[11] P. Pérez-Fernández, J. M. Arias, J. E. García-Ramos, and F. Pérez-Bernal, Finite-size corrections in the bosonic algebraic approach to two-dimensional systems, Phys. Rev. A **83**, 062125 (2011).
[12] M. Calixto, E. Romera, and R. del Real, Parity-symmetry-adapted coherent states and entanglement in quantum phase transitions of vibron models, J. Phys. A: Math. Theor. **45**, 365301 (2012).
[13] M. Calixto, R. del Real, and E. Romera, Husimi distribution and phase-space analysis of a vibron-model quantum phase transition, Phys. Rev. A **86**, 032508 (2012).
[14] F. de los Santos and E. Romera, Revival times at quantum phase transitions, Phys. Rev. A **87**, 013424 (2013).
[15] O. Castaños, M. Calixto, F. Pérez-Bernal, and E. Romera, Identifying the order of a quantum phase transition by means of Wehrl entropy in phase space, Phys. Rev. E **92**, 052106 (2015).
[16] P. Cejnar, M. Macek, S. Heinze, J. Jolie, and J. Dobeš, Monodromy and excited-state quantum phase transitions in integrable systems: Collective vibrations of nuclei, J. Phys. A: Math. Gen. **39**, L515 (2006).
[17] P. Cejnar and P. Stransky, Impact of quantum phase transitions on excited-level dynamics, Phys. Rev. E **78**, 031130 (2008).

[18] M. A. Caprio, P. Cejnar, and F. Iachello, Excited state quantum phase transitions in many-body systems, Ann. Phys.(NY) **323**, 1106 (2008).

[19] P. Stránský, M. Macek, and P. Cejnar, Excited-state quantum phase transitions in systems with two degrees of freedom: Level density, level dynamics, thermal properties, Ann. Phys. (NY) **345**, 73 (2014).

[20] P. Stránský, M. Macek, A. Leviatan, and P. Cejnar, Excited-state quantum phase transitions in systems with two degrees of freedom: II. Finite-size effects, Ann. Phys. (NY) **356**, 57 (2015).

[21] P. Stránský and P. Cejnar, Classification of excited-state quantum phase transitions for arbitrary number of degrees of freedom, Phys. Lett. A **380**, 2637 (2016).

[22] M. Macek, P. Stránský, A. Leviatan, and P. Cejnar, Excited-state quantum phase transitions in systems with two degrees of freedom. III. Interacting boson systems, Phys. Rev. C **99**, 064323 (2019).

[23] P. Cejnar, P. Stránský, M. Macek, and M. Kloc, Excited-state quantum phase transitions, J. Phys. A: Math. Theor. **54**, 133001 (2021).

[24] V. M. Bastidas, P. Pérez-Fernández, M. Vogl, and T. Brandes, Quantum Criticality and Dynamical Instability in the Kicked-Top Model, Phys. Rev. Lett. **112**, 140408 (2014).

[25] P. Pérez-Fernández, A. Relaño, J. M. Arias, P. Cejnar, J. Dukelsky, and J. E. García-Ramos, Excited-state phase transition and onset of chaos in quantum optical models, Phys. Rev. E **83**, 046208 (2011).

[26] T. Brandes, Excited-state quantum phase transitions in Dicke superradiance models, Phys. Rev. E **88**, 032133 (2013).

[27] M. A. Bastarrachea-Magnani, S. Lerma-Hernández, and J. G. Hirsch, Comparative quantum and semiclassical analysis of atom-field systems. I. Density of states and excited-state quantum phase transitions, Phys. Rev. A **89**, 032101 (2014).

[28] M. A. Bastarrachea-Magnani, S. Lerma-Hernández, and J. G. Hirsch, Comparative quantum and semiclassical analysis of atom-field systems. II. Chaos and regularity, Phys. Rev. A **89**, 032102 (2014).

[29] R. Puebla, M.-J. Hwang, and M. B. Plenio, Excited-state quantum phase transition in the Rabi model, Phys. Rev. A **94**, 023835 (2016).

[30] M. Kloc, P. Stránský, and P. Cejnar, Quantum quench dynamics in Dicke superradiance models, Phys. Rev. A **98**, 013836 (2018).

[31] Á. L. Corps and A. Relaño, Constant of Motion Identifying Excited-State Quantum Phases, Phys. Rev. Lett. **127**, 130602 (2021).

[32] J. Chavez-Carlos, B. López-del-Carpio, M. A. Bastarrachea-Magnani, P. Stránsky, S. Lerma-Hernández, L. F. Santos, and J. G. Hirsch, Quantum and Classical Lyapunov Exponents in Atom-Field Interaction Systems, Phys. Rev. Lett. **122**, 024101 (2019).

[33] P. Pérez-Fernández, A. Relaño, J. M. Arias, J. Dukelsky, and J. E. García-Ramos, Decoherence due to an excited-state quantum phase transition in a two-level boson model, Phys. Rev. A **80**, 032111 (2009).

[34] Z.-G. Yuan, P. Zhang, S.-S. Li, J. Jing, and L.-B. Kong, Scaling of the Berry phase close to the excited-state quantum phase transition in the Lipkin model, Phys. Rev. A **85**, 044102 (2012).

[35] W. Kopylov and T. Brandes, Time delayed control of excited state quantum phase transitions in the Lipkin-Meshkov-Glick model, New J. Phys. **17**, 103031 (2015).

[36] Q. Wang and F. Pérez-Bernal, Excited-state quantum phase transition and the quantum-speed-limit time, Phys. Rev. A **100**, 022118 (2019).

[37] Q. Wang and F. Pérez-Bernal, Probing an excited-state quantum phase transition in a quantum many-body system via an out-of-time-order correlator, Phys. Rev. A **100**, 062113 (2019).

[38] F. Pérez-Bernal and F. Iachello, Algebraic approach to two-dimensional systems: Shape phase transitions, monodromy, and thermodynamic quantities, Phys. Rev. A **77**, 032115 (2008).

[39] D. Larese and F. Iachello, A study of quantum phase transitions and quantum monodromy in the bending motion of non-rigid molecules, J. Mol. Struct. **1006**, 611 (2011).

[40] D. Larese, F. Pérez-Bernal, and F. Iachello, Signatures of quantum phase transitions and excited state quantum phase transitions in the vibrational bending dynamics of triatomic molecules, J. Mol. Struct. **1051**, 310 (2013).

[41] J. Khalouf-Rivera, F. Pérez-Bernal, and M. Carvajal, Excited state quantum phase transitions in the bending spectra of molecules, J. Quant. Spectrosc. Radiat. Transfer **261**, 107436 (2021).

[42] B. Dietz, F. Iachello, M. Miski-Oglu, N. Pietralla, A. Richter, L. von Smekal, and J. Wambach, Lifshitz and excited-state quantum phase transitions in microwave Dirac billiards, Phys. Rev. B **88**, 104101 (2013).

[43] L. Zhao, J. Jiang, T. Tang, M. Webb, and Y. Liu, Dynamics in spinor condensates tuned by a microwave dressing field, Phys. Rev. A **89**, 023608 (2014).

[44] P. Feldmann, C. Klempt, A. Smerzi, L. Santos, and M. Gessner, Interferometric Order Parameter for Excited-State Quantum Phase Transitions in Bose-Einstein Condensates, Phys. Rev. Lett. **126**, 230602 (2021).

[45] J. Cabedo, J. Claramunt, and A. Celi, Dynamical preparation of stripe states in spin-orbit-coupled gases, Phys. Rev. A **104**, L031305 (2021).

[46] F. Pérez-Bernal and O. Álvarez-Bajo, Anharmonicity effects in the bosonic U(2)-SO(3) excited-state quantum phase transition, Phys. Rev. A **81**, 050101 (2010).

[47] G. P. Berman and F. M. Izrailev, The Fermi-Pasta-Ulam problem: Fifty years of progress, Chaos **15**, 015104 (2005).

[48] A. L. Burin, A. O. Maksymov, M. Schmidt, and I. Y. Polishchuk, Chaotic dynamics in a quantum Fermi-Pasta-Ulam problem, Entropy **21**, 51 (2019).

[49] R. F. Casten, N. V. Zamfir, and D. S. Brenner, Universal Anharmonic Vibrator Description of Nuclei and Critical Nuclear Phase Transitions, Phys. Rev. Lett. **71**, 227 (1993).

[50] B. Monserrat, N. D. Drummond, and R. J. Needs, Anharmonic vibrational properties in periodic systems: Energy, electron-phonon coupling, and stress, Phys. Rev. B **87**, 144302 (2013).

[51] M. S. Child and L. Halonen, Overtone frequencies and intensities in the local mode picture, Adv. Chem. Phys. **57**, 1 (1984).

[52] M. E. Kellman, On the equivalence of the normal and local mode representations, J. Chem. Phys. **85**, 6242 (1986).

[53] M. E. Kellman and V. Tyng, The dance of molecules: New dynamical perspectives on highly excited molecular vibrations, Acc. Chem. Res. **40**, 243 (2007).

[54] F. Iachello and S. Oss, Algebraic approach to molecular spectra: Two dimensional problems, J. Chem. Phys. **104**, 6956 (1996).

[55] F. Iachello, F. Pérez-Bernal, and P. H. Vaccaro, A novel algebraic scheme for describing nonrigid molecules, Chem. Phys. Lett. **375**, 309 (2003).

[56] F. Pérez-Bernal, L. F. Santos, P. H. Vaccaro, and F. Iachello, Spectroscopic signatures of nonrigidity: Algebraic analyses of infrared and Raman transitions in nonrigid species, Chem. Phys. Lett. **414**, 398 (2005).

[57] F. Iachello and F. Pérez-Bernal, Bending vibrational modes of ABBA molecules: Algebraic approach and its classical limit, Mol. Phys. **106**, 223 (2008).

[58] F. Pérez-Bernal and L. Fortunato, Phase diagram of coupled benders within a U(3) × U(3) algebraic approach, Phys. Lett. A **376**, 236 (2012).

[59] D. Larese, M. A. Caprio, F. Pérez-Bernal, and F. Iachello, A study of the bending motion in tetratomic molecules by the algebraic operator expansion method, J. Chem. Phys. **140**, 014304 (2014).

[60] M. Sánchez-Castellanos, R. Lemus, M. Carvajal, F. Pérez-Bernal, and J. M. Fernández, A study of the Raman spectrum of CO_2 using an algebraic approach, Chem. Phys. Lett. **554**, 208 (2012).

[61] M. Sánchez-Castellanos, R. Lemus, M. Carvajal, and F. Pérez-Bernal, The potential energy surface of CO_2 from an algebraic approach, Int. J. Quantum Chem. **112**, 3498 (2012).

[62] R. Lemus, M. Sánchez-Castellanos, F. Pérez-Bernal, J. M. Fernández, and M. Carvajal, Simulation of the Raman spectra of CO_2: Bridging the gap between algebraic models and experimental spectra, J. Chem. Phys. **141**, 054306 (2014).

[63] M. Bermúdez-Montaña, M. Carvajal, F. Pérez-Bernal, and R. Lemus, An algebraic alternative for the accurate simulation of CO_2 Raman spectra, J. Raman Spectrosc. **51**, 569 (2020).

[64] W. Quapp and B. P. Winnewisser, What you thought you already knew about the bending motion of triatomic molecules, J. Math. Chem. **14**, 259 (1993).

[65] R. N. Dixon, Higher vibrational levels of a bent triatomic molecule, Trans. Faraday Soc. **60**, 1363 (1964).

[66] M. S. Child, Quantum states in a champagne bottle, J. Phys. A: Math. Gen. **31**, 657 (1998).

[67] M. Winnewisser, B. P. Winnewisser, I. R. Medvedev, F. C. De Lucia, S. C. Ross, and L. M. Bates, The hidden kernel of molecular quasi-linearity: Quantum monodromy, J. Mol. Struct. **798**, 1 (2006).

[68] L. M. Bates, Monodromy in the champagne bottle, Z. Angew. Math. Phys. **42**, 837 (1991).

[69] R. Cushman and J. J. Duistermaat, The quantum mechanical spherical pendulum, Bull. Am. Math. Soc. **19**, 475 (1988).

[70] M. S. Child, T. Weston, and J. Tennyson, Quantum monodromy in the spectrum of H_2O and other systems: New insight into the level structure of quasi-linear molecules, Mol. Phys. **96**, 371 (1999).

[71] B. P. Winnewisser, M. Winnewisser, I. R. Medvedev, M. Behnke, F. C. De Lucia, S. C. Ross, and J. Koput, Experimental Confirmation of Quantum Monodromy: The Millimeter Wave Spectrum of Cyanogen Isothiocyanate NCNCS, Phys. Rev. Lett. **95**, 243002 (2005).

[72] N. F. Zobov, S. V. Shirin, O. L. Polyansky, J. Tennyson, P.-F. Coheur, P. F. Bernath, M. Carleer, and R. Colin, Monodromy in the water molecule, Chem. Phys. Lett. **414**, 193 (2005).

[73] B. P. Winnewisser, M. Winnewisser, I. R. Medvedev, F. C. De Lucia, S. C. Ross, and J. Koput, Analysis of the FASSST rotational spectrum of NCNCS in view of quantum monodromy, Phys. Chem. Chem. Phys. **12**, 8158 (2010).

[74] M. Winnewisser, B. P. Winnewisser, F. C. De Lucia, D. W. Tokaryk, S. C. Ross, and B. E. Billinghurst, Pursuit of quantum monodromy in the far-infrared and mid-infrared spectra of NCNCS using synchrotron radiation, Phys. Chem. Chem. Phys. **16**, 17373 (2014).

[75] N. J. Reilly, P. B. Changala, J. H. Baraban, D. L. Kokkin, J. F. Stanton, and M. C. McCarthy, Communication: The ground electronic state of Si_2C: Rovibrational level structure, quantum monodromy, and astrophysical implications, J. Chem. Phys. **142**, 231101 (2015).

[76] J. Khalouf-Rivera, M. Carvajal, L. F. Santos, and F. Pérez-Bernal, Calculation of transition state energies in the HCN-HNC isomerization with an algebraic model, J. Phys. Chem. A **123**, 9544 (2019).

[77] L. Fortunato and L. Sartori, Detailed analysis of quantum phase transitions within the u(2) algebra, Commun. Theor. Phys. **54**, 589 (2010).

[78] J. Gamito, J. Khalouf-Rivera, J. M. Arias, P. Pérez-Fernández, and F. Pérez-Bernal, Excited-state quantum phase transitions in the anharmonic Lipkin-Meshkov-Glick model I: Static aspects, arXiv:2202.11413.

[79] J. Gamito, J. Khalouf-Rivera, J. M. Arias, P. Pérez-Fernández, and F. Pérez-Bernal, Excited-state quantum phase transitions in the anharmonic Lipkin-Meshkov-Glick model II: Dynamic aspects (unpublished).

[80] A. Relaño, C. Esebbag, and J. Dukelsky, Excited-state quantum phase transitions in the two-spin elliptic Gaudin model, Phys. Rev. E **94**, 052110 (2016).

[81] P. Stránský, P. Cejnar, and R. Filip, Stabilization of product states and excited-state quantum phase transitions in a coupled qubit-field system, Phys. Rev. A **104**, 053722 (2021).

[82] Á. L. Corps and A. Relaño, Energy cat states induced by a parity-breaking excited-state quantum phase transition, arXiv:2201.03976.

[83] K. Yamada and M. Winnewisser, A parameter to quantify molecular quasilinearity, Z. Naturforsch. A **31**, 139 (1976).

[84] J. H. Baraban, P. B. Changala, G. C. Mellau, J. F. Stanton, A. J. Merer, and R. W. Field, Spectroscopic characterization of isomerization transition states, Science **350**, 1338 (2015).

[85] L. F. Santos and F. Pérez-Bernal, Structure of eigenstates and quench dynamics at an excited-state quantum phase transition, Phys. Rev. A **92**, 050101(R) (2015).

[86] L. F. Santos, M. Távora, and F. Pérez-Bernal, Excited-state quantum phase transitions in many-body systems with infinite-range interaction: Localization, dynamics, and bifurcation, Phys. Rev. A **94**, 012113 (2016).

[87] F. Pérez-Bernal and L. F. Santos, Effects of excited state quantum phase transitions on system dynamics, Fortschr. Phys. **65**, 1600035 (2017).

[88] F. Evers and A. D. Mirlin, Anderson transitions, Rev. Mod. Phys. **80**, 1355 (2008).

[89] F. M. Izrailev, Simple models of quantum chaos: Spectrum and eigenfunctions, Phys. Rep. **196**, 299 (1990).

[90] V. Zelevinsky, B. A. Brown, N. Frazier, and M. Horoi, The nuclear shell model as a testing ground for many-body quantum chaos, Phys. Rep. **276**, 85 (1996).

[91] J. Khalouf-Rivera, M. Carvajal, and F. Pérez-Bernal, Quantum fidelity susceptibility in excited state quantum phase transitions: Application to the bending spectra of nonrigid molecules, SciPost Phys. **12**, 002 (2022).

[92] M. A. Nielsen and I. L. Chuang, *Quantum Computation and Quantum Information*, 10th ed. (Cambridge University Press, New York, 2011).

[93] P. Zanardi and N. Paunković, Ground state overlap and quantum phase transitions, Phys. Rev. E **74**, 031123 (2006).

[94] S.-J. Gu, Fidelity approach to quantum phase transitions, Int. J. Mod. Phys. B **24**, 4371 (2010).

[95] W.-L. You, Y.-W. Li, and S.-J. Gu, Fidelity, dynamic structure factor, and susceptibility in critical phenomena, Phys. Rev. E **76**, 022101 (2007).

[96] T. LeBlond, D. Sels, A. Polkovnikov, and M. Rigol, Universality in the onset of quantum chaos in many-body systems, Phys. Rev. B **104**, L201117 (2021).